International Journal of Hydrogen Energy 95 (2024) 1183–1193

Contents lists available at ScienceDirect

International Journal of Hydrogen Energy

journal homepage: www.elsevier.com/locate/he

Modelling of green ammonia production based on solid oxide cells as electrolyser and oxygen separator for Haber-Bosch loop decarbonization

Fiammetta Rita Bianchi *, Barbara Bosio

Department of Civil, Chemical and Environmental Engineering (DICCA), University of Genoa, Via Opera Pia 15, 16145, Genoa, Italy

ARTICLE INFO

Handling Editor: Ibrahim Dincer

Keywords:
Power-to-Ammonia
Hydrogen carrier
Solid oxide cells
Oxygen concentrator
Haber-Bosch loop
Process decarbonization

ABSTRACT

Ammonia is a well-known chemical and a rising candidate as hydrogen carrier. Nevertheless, its synthesis process decarbonization is a preliminary target. Since the Haber-Bosch loop is still the best path guaranteeing a high yield and capacity, alternative hydrogen and nitrogen upstream production steps have to be identified. Based on the water electrolysis, Power-to-Ammonia application allows for coupling the high performing traditional production process with renewables. This configuration would minimise the environmental impacts and make a decentralised local production feasible; nevertheless, its competitiveness strictly depends on reducing the electricity demand. Looking for low consumption electrolysis technologies, the work presents high-temperature solid oxide cells as one of the most competitive solutions showing a double operation, as hydrogen generator and as oxygen concentrator, which leads to H_2–N_2 mixture synthesis with a low energy demand (~8.5 kWh/kg NH_3) by optimizing the heat recovery and simplifying the plant design.

1. Introduction

Ammonia is one of the most common industrial chemicals which is involved in the manufacture of several products such as fertilizers, plastics, explosives, textiles, pesticides and dyes. Recently it has been proposed as an alternative energy carrier in view of its higher volumetric energy density, easier transport and safer storage than hydrogen, with applications as fuel for both internal combustion engines and fuel cells [1–4]. The state-of-art industrial process consists of the Haber-Bosch loop which allows a quite pure ammonia production (>99%) from hydrogen and nitrogen. Nevertheless, it has a significant energy consumption due to N_2 strong triple bond, requiring high temperatures (300–500 °C) and pressures (100–450 bar) to favour the reaction kinetics [5]. It is also characterised by high GHG emissions deriving commonly hydrogen from hydrocarbons (e.g., Methane-to-Ammonia application through natural gas steam reforming and Coal-to-Ammonia application through coal gasification) [6].

Ammonia production decarbonization can be achieved by: (i) avoiding traditional fossil fuel use, (ii) exploiting renewables as energy sources, (iii) identifying alternative processes for H_2/N_2 dissociation at milder working conditions and (iv) introducing innovative reactants which substitute the molecular nitrogen [7–10].

The first two points allow still the traditional Haber-Bosch loop use but coupled with more eco-friendly upstream steps resulting in Power-to-Ammonia and Biomass-to-Ammonia. They are characterised by a Technological Readiness Level (TRL) of 5–8, showing quite competitive performances with respect to traditional processes [11,12]. Power-to-Ammonia plants permit to minimise GHG emissions and obtain good efficiencies based on an electrolysis module and an air separation unit; on the other hand, they have a high electric consumption for the water dissociation and require proper storage systems in case of coupling with renewables to guarantee an ammonia continuous production [10,13,14]. Both Low-Temperature cells (LT cells) and High-Temperature cells (HT cells) have been proposed: the first are more mature technologies reaching a commercial size up to 1 MW/stack with lower capital costs (420–1200 €/kW of LT cells vs. 2000–4000 €/kW of HT cells) and longer lifetimes (10 years of LT cells vs. 5 years of HT cells), but the second ones have higher performances (4.5–6.5 kWh/Nm^3 H_2 of LT cells vs. 3.7–4 kWh/Nm^3 H_2 of HT cells) [15–17]. Here, from the economic point of view, the best electrolyser choice is strictly correlated to the electricity cost [18]. Another possible source of hydrogen is the syngas derived from biomass through thermochemical treatments. Despite resulting in a carbon neutral process, Biomass-to-Ammonia solution is characterised by significant consumption for the hydrogen purification (i.e., carbon capture steps); it is convenient just where low-cost biomass and animal waste can be used

* Corresponding author.
E-mail address: fiammettarita.bianchi@unige.it (F.R. Bianchi).

https://doi.org/10.1016/j.ijhydene.2024.07.047
Received 23 March 2024; Received in revised form 22 June 2024; Accepted 4 July 2024
Available online 11 July 2024
0360-3199/© 2024 The Authors. Published by Elsevier Ltd on behalf of Hydrogen Energy Publications LLC. This is an open access article under the CC BY license (http://creativecommons.org/licenses/by/4.0/).

for ammonia and fertiliser production in isolated zones [12,19]. The system optimization is understudied proposing more efficient biomass treatments, such as pyrolysis and sorption-enhanced gasification [20,21].

Processes alternative to the Haber-Bosch loop are also understudied; however, all have a TRL still lower than 4. The most promising solution consists of the ammonia production through electrolytic cells fed directly by H_2 and N_2 or their sources, such as water or methane and air respectively. In this case the reagent generation and the ammonia synthesis occur in a single unit, making it suitable for an ammonia decentralised production [22]. Under an electrolysis mode, the cells require an external electric power (around 0.6–1 V/cell) and temperatures ranging from room conditions to a maximum of 750 °C (higher values would lead to the ammonia dissociation) as a function of electrolyte materials [23]. The basic operation involves a proton or a hydroxide ion exchange electrolyte [24,25], while the nitride ion conductive electrolytes are more rarely applied [8]. A peculiar operation characterises anionic conductive electrolyte-based cells, which can work in both electrolysis mode, where the water dissociation favours NH_3 formation [26], and in fuel cell mode, where a wet air oxidant allows for producing NH_3 simultaneously with the electricity generation [27].

Alternatively, nitrate-containing wastewaters can be a nitrogen

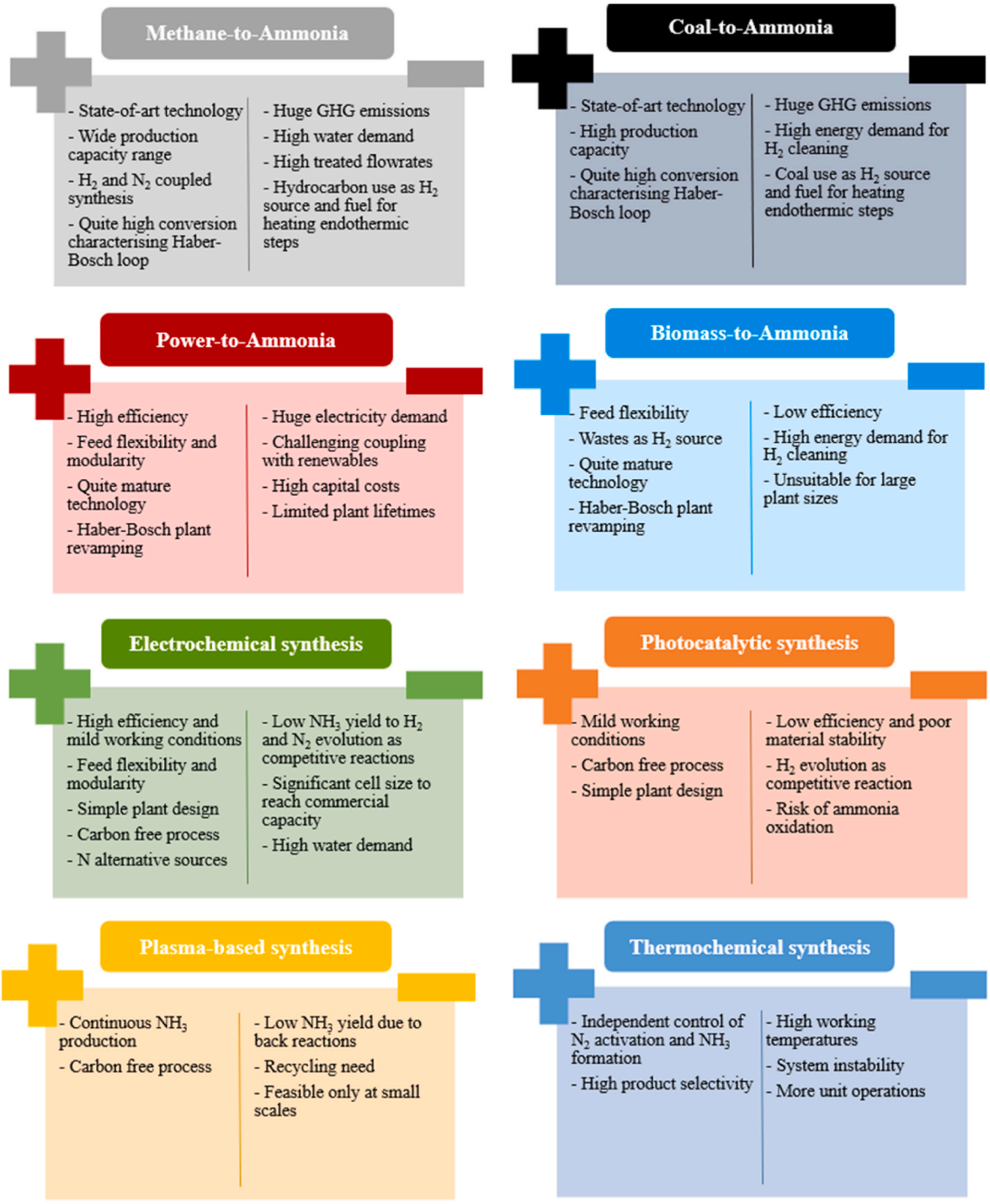

Fig. 1. Comparison of pros (+) and cons (−) of green ammonia production processes with respect to traditional plants. (For interpretation of the references to colour in this figure legend, the reader is referred to the Web version of this article.)

source for the ammonia synthesis through the electrocatalytic denitrification [28]. Its production rate is higher than the electrolytic cell values; nevertheless, it needs high nitrate concentrations limiting the useable wastewaters or requiring the treated flowrate increase [29,30]. In this framework, the most recent works aim at the electrocatalyst material optimization to increase the ammonia production, reduce the degradation issues and allow the use of nitrogen-containing compounds instead of air [31–33].

The photocatalytic synthesis consists of semiconductor materials driving the simultaneous N_2 photoreduction and H_2O photooxidation to produce ammonia at room conditions [8]; low efficiency, selectivity and stability are the main technical constraints [34,35], requiring a detailed engineering of the process to favour an industrial application [36].

The plasma-based synthesis involves the use of an electrically ionized gas, generated by microwave or dielectric barrier discharge systems, to favour the nitrogen dissociation and the ammonia formation under mild working conditions [8,37,38]. As downside, the residence time is minimised to penalise several possible back reactions leading to a low conversion rate and the unreacted gas recycling, which needs the used catalyst optimization [39,40]. Alternatively, a Plasma Nitrogen Oxidation coupled with Catalytic Reduction to Ammonia (PNOCRA) application has been proposed where N_2 from air is oxidized to NO_x using a plasma reactor and further adsorbed on a Lean NOx Trap (LNT) bed, which is then regenerated by feeding hydrogen and here obtaining NH_3 [41].

Finally, the thermochemical cycle process, also called Chemical Looping Ammonia Production (CLAP), requires a first reactor where a nitrogen-rich stream favours the nitridation of the carrier (usually a pure metal or its derivatives), and a second reactor where the carrier is reduced back to its initial state under a hydrogen-rich environment whilst forming ammonia [5]. Indeed, decoupling the nitrogen activation and the ammonia formation makes the synthesis easier. On the other hand, this loop has a high heat demand, reaching also more than 1000 °C, only partially satisfied by an optimised thermal balance between the exothermic oxidation and the endothermic reduction. A process efficiency increase is attended through a careful choice of nitrogen carriers [42–44].

Considering the several constraints of these new technologies, their combination has been also discussed in order to take the main advantages and mitigate the negative aspects such as high working temperatures and possible competitive reactions [5,45–47].

Available processes for the ammonia production are summarised in Fig. 1, comparing the state-of-art solutions with more sustainable technologies.

According to the previous considerations, Power-to-Ammonia approach results in the most promising industrial solution for the Haber-Bosch loop revamping. Nevertheless, there are still several unresolved key-points, and all available electrolysis technologies should be evaluated in more detail by underlining peculiarities, potentialities, drawbacks and possible plant flowsheets. Despite of high performances, the solid oxide cells have been studied in still few research works which have investigated their application as electrolysers for the green ammonia synthesis or as reversible fuel cells using ammonia energy vector for the renewable energy storage [48–51].

The present work reports a feasibility analysis of the green ammonia production through solid oxide cells compared to Methane-to-Ammonia, discussing the possible flowsheets. Indeed, the cells can work as: (i) a steam electrolyser for the hydrogen generation, (ii) an electrochemical air separation unit for the oxygen concentration and the nitrogen separation, (iii) a technology combining these two previous functionalities allowing the direct production of the H_2/N_2 reactant mixture. If the first operation has almost reached a mature technological level [52], the electrochemical air separation unit is a quite new solution with the first lab-scale tests [53,54], requiring some preliminary modelling studies to validate the use. All proposed plant designs are characterised in terms of material and energy flows comparing the water consumption, the electricity demand and the heat requirements at an ammonia fixed production capacity, differently from the previous references where a single cell operation has been usually analysed [18,55–58]. In addition to discussing the global plant performance, the cell specific operation and design are underlined with a focus on strengths and constraints when working in an endothermic or an exothermic mode.

2. Theoretical background and process development

2.1. Ammonia synthesis

Ammonia formation is an equilibrium exothermic reaction (Eq. (1)), which would occur at high pressures and low temperatures. Nevertheless, the system needs up to 300–600 °C to overcome the kinetic limits, resulting in a NH_3 insufficient production rate for a commercial scale since the thermodynamics favours the opposite reaction (i.e., hydrogen and nitrogen formation). This issue is solved using proper catalysts, usually based on iron or ruthenium, and introducing a cyclic operation where the NH_3 produced low amount is separated and the H_2/N_2 unreacted mixture is recirculated to permit its further conversion [5]. A refrigeration unit permits to divide the liquid ammonia which is so ready for the storage below – 34 °C at an atmospheric pressure [59].

$$0.5N_2 + 1.5H_2 \leftrightarrow NH_3 \ (\Delta H^0 = -46\ kJ/mol) \quad \text{Eq. 1}$$

2.2. Solid oxide cell operation

Solid Oxide Cell (SOC) technology is based on ceramic and cermet materials working at high temperatures to favour the ion migration within a solid phase. In Solid Oxide Electrolysis Cells (SOECs), the water electrochemical dissociation (Eq. (2)) develops at the cathode through its reduction into molecular hydrogen and oxygen ion which migrates across the anionic conductive electrolyte to give molecular oxygen at the anode (Eq. (3)). This process is characterised by an electricity consumption lower than 4 kWh/Nm^3 H_2 since a fraction of the required energy is provided as heat [15]. According to these reactions, the cell can be also used as an oxygen separator: from the cathode generating $O^=$ ions to the anode releasing pure O_2. Indeed, 1 mol of oxygen is obtained simultaneously at the production of 2 mol of hydrogen (Eq. (4)).

$$H_2O + 2e^- \rightarrow H_2 + O^= \ cathode \quad \text{Eq. 2}$$

$$O^= \rightarrow 0.5O_2 + 2e^- \ anode \quad \text{Eq. 3}$$

$$H_2O \rightarrow H_2 + 0.5O_2 \ \ (\Delta H^0 = 285\ kJ/mol) \ global\ cell \quad \text{Eq. 4}$$

Alternatively the cell can work just as an electrochemical Air Separation Unit (e-ASU) by feeding air at the cathode and obtaining pure oxygen at the anode (Eq. (5) and Eq. (6)).

$$O_2 + 4e^- \rightarrow 2O^= \ cathode \quad \text{Eq. 5}$$

$$2O^= \rightarrow O_2 + 4e^- \ anode \quad \text{Eq. 6}$$

Under both an electrolysis and an e-ASU operation, the gas production/separation rate depends linearly on the applied external load according to Faraday law. Higher current densities favour the process but also mean a higher required power in order to overcome all material resistances to the current flux, according to Eq. (7).

$$P_{el} = VJAn = VN_{gas}zF \ with \ V = V_{eq} + \sum V_p \quad \text{Eq. 7}$$

Where P_{el} is the electric power, V the single cell voltage, J the current density as absolute value, A the single cell active area, n the stacked cell number, N_{gas} the produced gas flowrate (i.e., H_2 under electrolysis and O_2 under e-ASU), z the transferred charge, F the Faraday constant. The cell voltage is the sum of the equilibrium value V_{eq} and a series of overpotentials V_p correlated to the ion migration, the reaction

development and the gas transport resistances.

The cell thermal behaviour is also strictly correlated with the current density, since the charge flux releases heat due to Joule effect leading to a temperature increase in an adiabatic system. This is true under e-ASU mode, differently in the electrolysis operation the actual temperature profile depends on a balance between the exothermic Joule effect and the endothermic water dissociation (Eq. (8)). In order to minimise the thermal stresses and simplify the electrolyser management, the thermoneutral condition is commonly applied permitting an almost isothermal behaviour reached at a voltage equal to the thermoneutral potential V_{th} (at higher values the system results exothermic, at lower ones endothermic). It is noteworthy that the efficiency maximises at such a point since all the provided energy is effectively used to produce hydrogen without dissipations due to Joule effect [60].

$$P_{th} = N_{H_2}\Delta H_{H_2/H_2O} - P_{el} = (N_{H_2} zFV_{th} - N_{H_2} zFV_{SOEC}) \; defining \; V_{th} = \frac{\Delta H_{H_2/H_2O}}{zF} \quad \text{Eq. 8}$$

Where P_{th} is the thermal power characterising the electrolysis mode, $\Delta H_{H_2/H_2O}$ the water dissociation reaction enthalpy which has a low thermal dependence at common working temperatures resulting in a constant V_{th} equal to ~1.29 V, V_{SOEC} the single electrolysis cell voltage.

2.3. Plant design

Four plant designs were considered starting from the Methane-to-Ammonia configuration, taken as the reference, to the Power-to-Ammonia processes based on solid oxide cells under three operations: (i) a solid oxide electrolyser coupled with an air separation unit, (ii) a solid oxide electrolyser coupled with an electrochemical air separation unit, (iii) a solid oxide electrolyser working also as an oxygen concentrator.

The first case-study, following defined as "*SR + ASU + HB*", consists of three sub-processes: (i) natural gas Steam Reforming for the hydrogen generation, (ii) Air Separation Unit for the nitrogen separation and (iii) Haber-Bosh loop including the synthesis reactor, the refrigeration unit to remove liquid ammonia and the reactant recirculation (Fig. 2). Natural gas at 25 °C and 15 bar is compressed and heated before the steam reforming reactor working up to 980 °C and 35 bar to have an almost complete conversion of the methane [61,65]. A steam to carbon equal to 4.7 avoids the coke formation requiring the steam generation at 360 °C and 35 bar through the natural gas combustion, which increases the effective fuel demand of the plant. The produced syngas is cooled down to 200 °C and converted in a water gas shift reactor to maximize the hydrogen yield. Following there are several purification steps to remove all oxidized compounds which poison the ammonia synthesis catalyst. After reducing temperatures, the condensed water is easily separated and the CO_2 is removed through the amine absorption (capture efficiency of ~95%, reboiler duty of ~0.98 kWh_{th}/kg CO_2, pump and compressor electric work of ~0.09 kWh_{el}/kg CO_2 [62]). Finally, a Sabatier reactor at 300 °C and 35 bar allows for removing any traces of CO and CO_2 consuming a fraction of hydrogen yet. The produced methane is not a dangerous compound within the Haber-Bosch loop if in low amounts. After the remaining water condensation, the H_2-rich stream is mixed with the nitrogen produced by the air separation unit up to a H_2/N_2 molar ratio equal to around 3. In commercial plants the air cryogenic distillation is usually applied permitting nitrogen at high purity levels with quite low consumption [63]. Nevertheless, the pressure swing adsorption technology (energy consumption of ~0.3 kWh_{el}/kg N_2 [64]) results in the most suitable solution in this analysis comparing the Methane-to-Ammonia process with the Power-to-Ammonia solution in view of a lower available capacity of the second. The Haber-Bosh loop consists of a series of compressors and heaters to reach 500 °C and 200 bar within the magnetite-based synthesis reactor [5]. The outlet product is cooled down to the ammonia boiling temperature and expanded below 30 bar to remove an almost pure liquid ammonia (>99%) and recirculate unreacted gases after their re-heating and re-compression. A purge is required to avoid inert accumulation (methane above all). The liquid ammonia is expanded further until 1.3 bar for a safe cryogenic storage [59].

The second case-study, following defined as "*SOEC + ASU + HB*", consists of three sub-processes: (i) Solid Oxide Electrolysis Cell for the hydrogen generation, (ii) Air Separation Unit for the nitrogen separation and (iii) Haber-Bosh loop (Fig. 3). Last two points are equal to the previous flowsheet, nevertheless in this case a pure H_2/N_2 mixture is fed to the loop allowing for the purge minimization (~50% reduction with respect to *SR-ASU-HB* case) and a higher pressure of the recycling stream (up to 95 bar). Referring to the H_2 synthesis, the solid oxide cell use simplifies significantly the plant involving just a module of stacked cells (active area of around 130 cm^2) and a heating step for the steam generation at high temperatures. The inlet pure steam is mixed with a fraction of the produced hydrogen-rich stream (~10%) to prevent the cathodic electrocatalyst oxidation. The pure oxygen, obtained as by-product, is partially recirculated (~50%) as the anodic sweeping gas already at high temperatures. Working at the thermoneutral potential (~1.29 V/cell) permits an isothermal behaviour at 750 °C and 1 bar. The steam utilization, defined as the water consumed on the fed amount, is

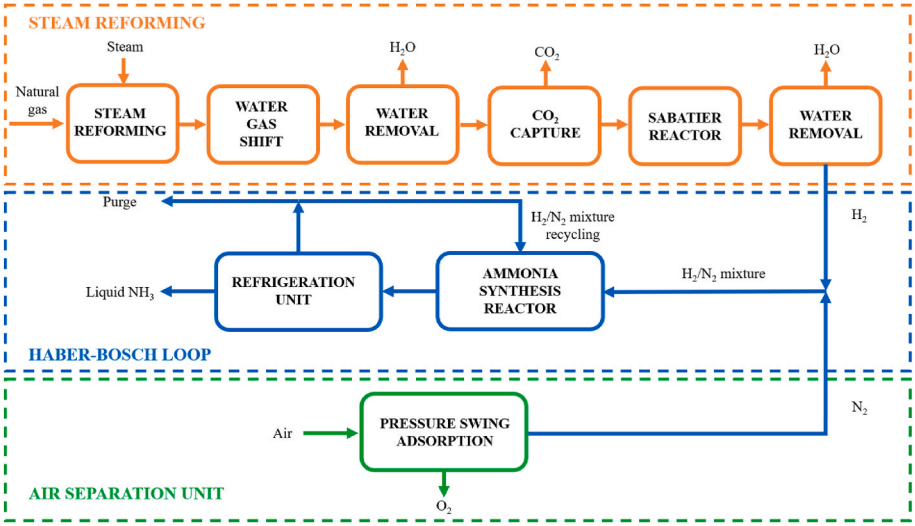

Fig. 2. Flowsheet of Steam Reforming + Air Separation Unit + Haber-Bosch loop (SR + ASU + HB) plant.

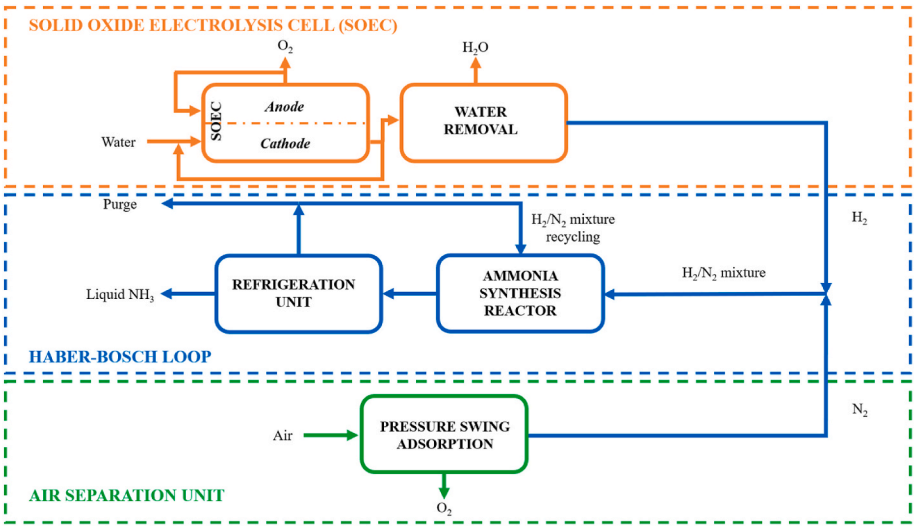

Fig. 3. Flowsheet of Solid Oxide Electrolysis Cell + Air Separation Unit + Haber-Bosch loop (SOEC + ASU + HB) plant.

usually fixed at around 90% to prevent starvation. The wet hydrogen cathodic product is cooled down to remove water before mixing with nitrogen derived from the pressure swing adsorption and feeding to the Haber-Bosch loop. All the required electricity for the different unit operations is provided by renewables to produce a "green ammonia".

Finally, the third and the fourth case-studies aim at a system further simplification involving the solid oxide cell technology for both the hydrogen generation and the oxygen separation upstream of the Haber-Bosh loop. Referring to "*SOEC + e-ASU + HB*" case (Fig. 4), two distinctive solid oxide cell modules are applied: the first working in electrolysis mode to generate H_2 at the cathode and O_2 by-product at the anode from steam fed to the cathode; the second working as electrochemical air separation unit to obtain N_2-rich stream at the cathode and pure O_2 by-product at the anode from air fed to the cathode. Fixed the inlet working conditions at 750 °C and 1 bar, the electrolyser works at the thermoneutral point with a steam conversion of around 90% while the e-ASU has an oxygen utilization of 98% (defined as the separated oxygen over the fed amount). A fraction of the produced oxygen is again recirculated as the anodic sweeping gas. Since e-ASU technology is an oxygen concentrator [66,67], the outlet cathodic N_2-rich stream contains argon, an inert, and a still small amount of oxygen which burns when mixed with H_2.

In "*SOEC + HB*" plant design (Fig. 5), a distinct air separation unit module is not necessary since feeding air directly to the electrolysis cells. The stacks are alternated in series with intermediate air burners. Here nitrogen is introduced into the cathodic synthesis gas burning the oxygen with a part of hydrogen generated by the previous electrolysis unit and releasing steam for the following one (i.e., obtaining N_2/H_2O mixture as the cell cathodic feed). In other terms, the solid oxide cells can be seen as an oxygen separator from the cathode forming oxygen ions by water (Eq. (2)) to the anode releasing molecular oxygen (Eq. (3)), directly mixing H_2 and N_2 in this configuration [55]. The combustion heat balances the hydrogen fraction loss and the electricity requirement for its following re-synthesis; indeed, it permits to operate below the thermoneutral voltage using this external source to maintain an isothermal behaviour at ~750 °C. Therefore, the cells work at lower loads resulting in lower electric powers without operation penalizations due to the theoretical endothermic behaviour. This scheme is repeated until a stoichiometric gas with a H_2/N_2 molar ratio of around 3 can be provided to the ammonia synthesis loop. This stream contains argon as in *SOEC + e-ASU + HB* case, since the process separates selectively only nitrogen from oxygen through its combustion and migration within the solid electrolyte. Here a bit higher purge percentage is required in both of these two last plants using an oxygen concentrator instead of the

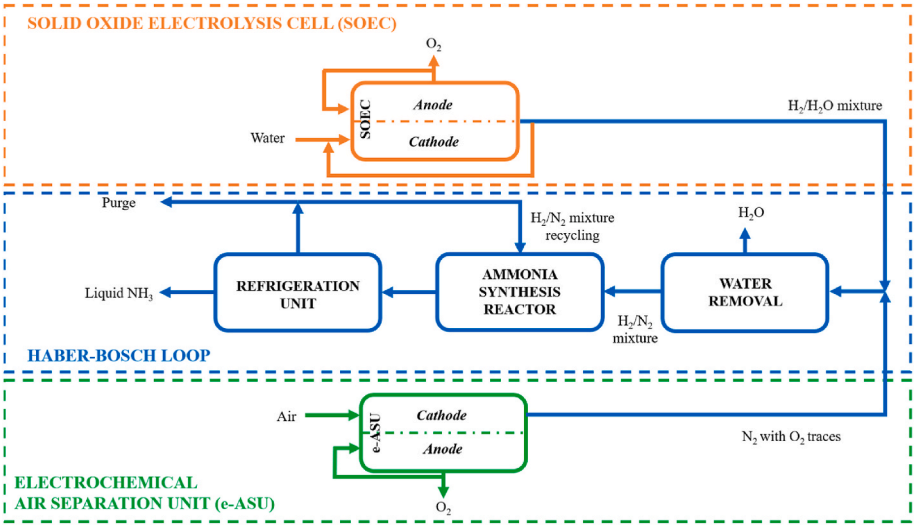

Fig. 4. Flowsheet of Solid Oxide Electrolysis Cell + electrochemical Air Separation Unit + Haber-Bosch loop (SOEC + e-ASU + HB) plant.

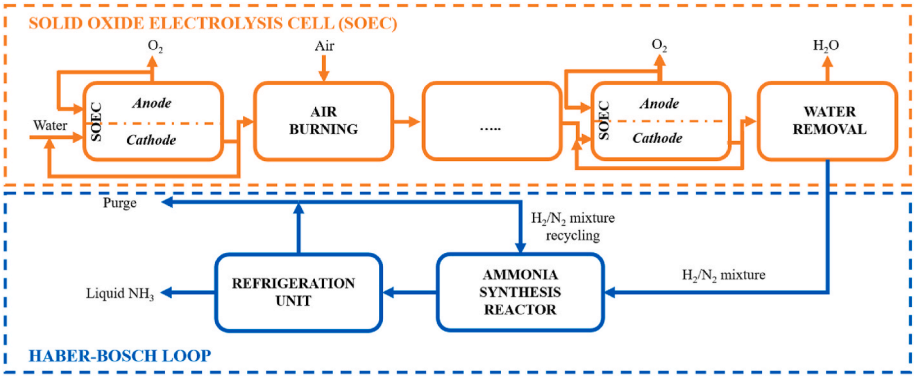

Fig. 5. Flowsheet of Solid Oxide Electrolysis Cell + Haber-Bosch loop (SOEC + HB) plant (note the whole succession of electrolysis and air burning steps is not here shown for graphical reasons).

pressure swing adsorption coupled with SOECs (14% increase).

2.4. Modelling assumptions and performance indexes

The previously described plant designs were modelled by a commercial process simulation software which solves material, energy and momentum balances. Equilibrium reactions, ideal heat exchanges and isentropic gas compressions were assumed. Focusing on the solid oxide cell technology, a simplified 0D version of SIMFC/SIMEC (SIMulation of Fuel Cells and Electrolysis Cells), an in house-built physics-based code, was integrated for the cell operation prediction. This model has been already widely described and validated on state-of-art solid oxide cell materials through experimental data comparison in authors' previous works [68–72]. Here Eq. (9) and Eq. (10) briefly summarise the electrochemical kinetics referring respectively to the electrolyser and the e-ASU, with all the parameters reported in Table 1. The main visible differences depend on the cell geometry considered for each specific operation: a cathode-supported cell for the electrolyser and an electrolyte-supported cell for the oxygen separator [73].

$$V_{SOEC} = V_{eq} + \gamma_{ohm_SOEC} T \exp\left(\frac{E_{a,ohm_SOEC}}{R_g T}\right) J + \frac{R_g T}{F}\sinh^{-1}\left[\frac{J}{2\gamma_{cat} y_{H_2}^{0.5} y_{H_2O}^{0.5} \exp\left(\frac{E_{a,cat}}{R_g T}\right)}\right] + \frac{R_g T}{2F}\sinh^{-1}\left[\frac{J}{2\gamma_{an} y_{O_2}^{0.25} \exp\left(\frac{E_{a,an}}{R_g T}\right)}\right] + \left|\frac{R_g T}{2F}\ln\left(\frac{1-\frac{J}{J_{lim,H_2O}}}{1+\frac{J}{J_{lim,H_2}}}\right)\right| \quad \text{Eq. 9}$$

Table 1
Kinetic parameters for electrolyser and e-ASU voltage calculation by SIMFC/SIMEC model [74].

Kinetic Parameter	Value				
Pre-exponential coefficient	γ_{ohm_SOEC} [$\Omega m^2/K$] $4 \bullet 10^{-11}$	γ_{cat} [A/m^2] $5 \bullet 10^{9}$	γ_{an} [A/m^2] $5 \bullet 10^{10}$	γ_{ohm_eASU} [$\Omega m^2/K$] $9 \bullet 10^{-11}$	γ_{eASU} [A/m^2] $5 \bullet 10^{10}$
Activation energy	E_{a,ohm_SOEC} [kJ/mol] 58.2	$E_{a,cat}$ [kJ/mol] 100	$E_{a,an}$ [kJ/mol] 120	E_{a,ohm_eASU} [kJ/mol] 58.2	$E_{a,eASU}$ [kJ/mol] 120

$$V_{eASU} = V_{eq} + \gamma_{ohm_eASU} T \exp\left(\frac{E_{a,ohm_eASU}}{R_g T}\right) J + \sum_{i}^{an,cat}\left\{\frac{R_g T}{2F}\sinh^{-1}\left[\frac{J}{2\gamma_{eASU} y_{O_2,i}^{0.25} \exp\left(\frac{E_{a,eASU}}{R_g T}\right)}\right] + \left|\frac{R_g T}{4F}\ln\left(1 \pm \frac{J}{J_{lim,O_2,i}}\right)\right|\right\} \quad \text{Eq. 10}$$

Where γ are the kinetic pre-exponential coefficients, T the temperature, E_a the activation energies, R_g the ideal gas constant, y the gas molar fractions, J_{lim} the limiting current densities.

The following performance indexes were applied to both the global plant and the single unit operations aiming at a feasibility analysis of ammonia alternative production paths. The specific electric E_{el} and heat E_{th} demands are defined as in Eq. (11) and Eq. (12) respectively, representing the consumed energy for the produced ammonia.

$$E_{el} = \frac{P_{el}}{N_{NH_3}} \quad \text{Eq. 11}$$

$$E_{th} = \frac{P_{th}}{N_{NH_3}} \quad \text{Eq. 12}$$

Where P_{el} and P_{th} are the electric duty and the heat, N_{NH_3} the ammonia outlet flowrate. The first index is always positive not considering power generators within the analysed systems, while the second assumes a positive value in case of endothermic unit operations and a negative value in the exothermic ones.

The total energy demand E_{tot} also includes the contribution due to fossil fuels in terms of their chemical energy in addition to the electric work (Eq. (13)).

$$E_{tot} = \frac{\sum P_{el} + N_{fuel} LHV_{fuel}}{N_{NH_3}} \quad \text{Eq. 13}$$

Where N_{fuel} is the fed fuel (i.e., natural gas) and LHV_{fuel} its Lower Heating Value.

The global process energy efficiency η is defined as the ratio of the energy contained in the produced ammonia to the energy provided to the system as both electricity and fuel chemical energy (Eq. (14)).

$$\eta = \frac{N_{NH_3} LHV_{NH_3}}{\sum P_{el} + N_{fuel} LHV_{fuel}} = \frac{LHV_{NH_3}}{E_{tot}} \quad \text{Eq. 14}$$

Where LHV_{NH_3} is the Lower Heating Value of ammonia.

3. Results and discussion

Industrial plants based on the natural gas steam reformer have generally a daily capacity from 200 to 500 ton for small scales to 2000–3000 ton for large scales. On the contrary, the Power-to-Ammonia application is currently designed to produce a lower amount, around 100 ton/d, in view of the available commercial electrolyser maximum capacity (despite 100 MW of attended future performance). For instance, the only long-term working plant in Peru exploits a 25 MW alkaline electrolyser and does not exceed a daily production of around 60–65 ton [12].

In this framework, the present work targets a prospective ammonia plant capacity of ~5 ton/h (i.e., ~120 ton/d) and compares reactant and energy consumption characterising the traditional process with respect to the proposed innovative solutions based on solid oxide cells (Table 2).

Referring to *SR + ASU + HB* case, it requires a feed of ~3.1 ton/h of natural gas and ~16.2 ton/h of water for the steam reforming reactor producing a syngas with 43 vol% of H_2. The content rises to 49 vol% and 94 vol% after the water gas shift and the purification steps (i.e., water condensation and CO_2 removal) respectively. Following, it decreases of ~17% after the methanation providing ~14,281 Nm^3/h with 6 vol% of CH_4 as the Haber-Bosch loop feed. In the case of solid oxide cell-based solutions, the water demand is lower (~10 tons/d), producing 11,200 Nm^3/h of pure H_2 through the electrolysis. Indeed, the steam reforming reactor requires a strongly oxidized environment to avoid the carbon deposition and separates the excess downstream through several condensation units. Differently, the electrolysis converts almost all the fed water directly into hydrogen under a high utilization of steam (~90%). Moreover, the hydrogen requirement for the ammonia synthesis is lower in Power-to-Ammonia plants since the hydrogen reactor conversion moves from ~22% using an upstream steam reformer to ~29% using an upstream SOEC due to the inert presence changing both the feed composition and the purged amount. In all plant designs the purges consist mainly of unreacted hydrogen and nitrogen with an ammonia loss always lower than 4 vol%. Nevertheless, *SR + ASU + HB* case contains also a 19 vol% of CH_4 due to Sabatier reactor, which results in a ~40% higher LHV (~8 kWh/kg vs. ~5 kWh/kg) permitting this mixture use as an additional energy source. Actually, methane could be removed through a cryogenic separation step with a further temperature-pressure variation before the Haber-Bosch loop [6]. This solution is not considered in the present study aiming at a plant design as compact as possible. It is noteworthy that there is a bit higher purged flowrate in *SOEC + e-ASU + HB* and *SOEC + HB* cases due to argon (~2 vol%).

Table 2
Inputs and outputs of ammonia production plant designs in terms of material and energy streams.

Parameter	CASE 1 *SR + ASU + HB*	CASE 2 *SOEC + ASU + HB*	CASE 3 *SOEC + e-ASU + HB*	CASE 4 *SOEC + HB*
Produced ammonia [ton/h]	5.2			
Ammonia purity degree [%]	>99			
Fed natural gas @ 25 °C-15 bar [ton/h]	3.3	–	–	–
Fed water @ 20 °C-1 bar [ton/h]	16.2	10.0	10.0	10.0
Required hydrogen [Nm^3/h]	13,334	11,200	11,200	11,200
Required nitrogen [Nm^3/h]	4443	3733	3733	3733
Produced pure oxygen [Nm^3/h]	1196	6605	6585	6605
Purged stream [Nm^3/h]	4774	1169	1214	1371
Electricity demand [MW_{el}]	10.61	43.73	44.30	44.99
Total specific energy consumption [kWh/kg NH_3]	10.43	8.37	8.45	8.66
CO_2 specific production [kg CO_2/kg NH_3]	1.38	–	–	–

The hydrogen content difference consequently varies the nitrogen demand, lower of ~710 Nm^3/h using solid oxide cells, in order to have a H_2/N_2 molar ratio always equal to around 3.

Pure oxygen is a high value by-product obtainable by the air separation unit and the steam electrolysis, here resulting in higher values when SOEC technology is used since both sources are present. In *SOEC + HB* case the oxygen can be completely burnt and separated within cells as ions, explaining a detected value equal to *SOEC + ASU + HB* plant. Differently *SOEC + e-ASU + HB* case is characterised by a bit smaller amount due to oxygen lost by its combustion when the N_2-rich stream is mixed with hydrogen upstream the loop.

Referring to the energy consumption, SOEC-based processes have a significant electricity demand which is always higher than *SR + ASU + HB* plant one. Indeed, the steam electrolysis represents alone up to ~81% of the total required electric work, the remaining fraction is due to Haber-Bosch loop and ASU when needed. In the traditional design, the hydrogen production including the steam reforming and the purification steps covers just the ~23% of the inlet demand. The power for the Haber-Bosch loop is quite similar in all flowsheets, obtaining a balance between a higher compression work on H_2/N_2 inlet mixture using an atmospheric solid oxide electrolyser (vs. 35 bar as inlet pressure in *SR + ASU + HB*) and a higher compression work for the recycling in *SR + ASU + HB* due to its higher flowrate (~40% difference) and lower pressure (30 bar vs. 95 bar). Comparing *SOEC + ASU + HB* and *SOEC + e-ASU + HB*, the electricity mismatch is mainly due to the nitrogen separation process as the electrolyser operation is identical. Since e-ASU technology has a low technological readiness level with only lab-scale results available, a precautionary consumption of ~2 kWh/Nm^3 of separated O_2 was considered despite that more promising performances are attended [53]. Here e-ASU is more energy consuming: 500 kW extra with respect to the pressure swing adsorption at an equal separation capacity of nitrogen. Looking at *SOEC + HB* case, a difference of around 2 MW is detected for the electrolyser demand due to the additional energy required to reconvert the hydrogen oxidized in intermediate burning steps (~34.5 MW vs. ~36.5 MW). This value balances fairly ASU consumption in *SOEC + ASU + HB* and *SOEC + e-ASU + HB* cases yet (1.4 MW and 1.9 MW respectively). Here *SOEC + HB* system allows for the plant design simplification avoiding an additional module devoted to the air separation, without a significant penalty on the energy consumption due to more reacted water.

Considering the specific total energy consumption, *SOEC + ASU + HB, SOEC + e-ASU + HB* and *SOEC + HB* plants are characterised by similar values resulting in 8.37 kWh/kg NH_3, 8.45 kWh/kg NH_3 and 8.66 kWh/kg NH_3 respectively. These are all lower than *SR + ASU + HB* case where 10.43 kWh/kg NH_3 is required including the electricity demand and the energy content of the used natural gas. With the aim of Haber-Bosch process decarbonization, these results are very competitive with other proposed commercial sustainable solutions involving low-temperature electrolysis cells (9–10 kWh/kg NH_3) and biomass gasification (>11 kWh/kg NH_3) as shown in Fig. 6 [12]. Looking at the energy efficiency, the best performance again characterises the SOEC-based plant designs obtaining ~60% with respect to ~50% in *SR + ASU + HB* case. It is noteworthy that further improvements are still possible by introducing new under-test solid oxide cells which should operate up to 25 bar reducing the compression work in the Haber-Bosch loop [75]. Another significant benefit is the CO_2 production minimization compared with ~1.38 kg CO_2/kg NH_3 or more in Methane-to-Ammonia plants and up to 4 kg CO_2/kg NH_3 in Coal-to-Ammonia ones. The Biomass-to-Ammonia configuration has quite similar values to those of natural gas-based plants, nevertheless the system can be considered carbon neutral [12].

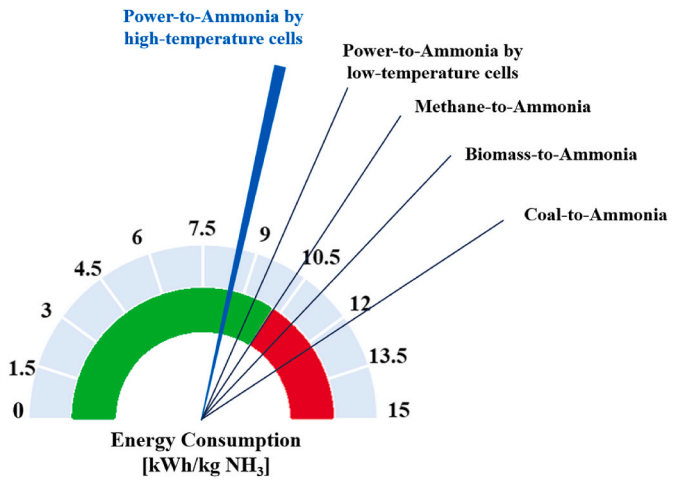

Fig. 6. Energy consumption comparison for state-of-art and more sustainable technologies based on Haber-Bosch loop.

Fig. 7 represents the specific energy consumption of all unit operations involved in the ammonia production plants. In Methane-to-Ammonia case, the electricity demand is mainly due to the compression work in the Haber-Bosch loop (~1.56 kWh_{el}/kg NH_3) and the pressure swing adsorption operation (~0.32 kWh_{el}/kg NH_3) for a total value of ~2.03 kWh_{el}/kg NH_3. The highest heat demand is correlated to hydrogen production steps, namely the steam reforming (~6.51 kWh_{th}/kg NH_3) and the CO_2 separation process (~1.35 kWh_{th}/kg NH_3). In *SOEC + ASU + HB* the highest electric work is reached by the steam electrolysis which requires a considerable amount for water electrochemical dissociation (~6.59 kWh_{el}/kg NH_3) as well as a heat source for high-temperature steam production (~1.85 kWh_{th}/kg NH_3). This last term can be partially balanced by a proper thermal management of cell modules exploiting hot outlet products. The system can recover also partially the heat from the exothermic ammonia synthesis reactor working at 500 °C (~-0.89 kWh_{th}/kg NH_3), which is one of the benefits of coupling high-temperature electrolysis cells with Haber-Bosch loop. Looking at *SOEC + e-ASU + HB* design, the results are quite similar except for the nitrogen separation step which has a higher electricity demand (~0.37 kWh_{el}/kg NH_3). Moreover, e-ASU cell module works at 750 °C resulting in a heat demand of ~0.20 kWh_{th}/kg NH_3. The worst detected performance for the electrolysis step characterises *SOEC + HB* plant: it reaches ~7.03 kWh_{el}/kg NH_3 due to the double reduction of a water fraction; it also requires more heat (~2.61 kWh_{th}/kg NH_3) to have an actual isothermal cell behaviour working below the thermoneutral point (i.e., single cell voltage lower than ~1.29 V). However, air burning intermediate steps can provide the heat for the stacks and a fraction for the inlet steam generation. The specific electric and heat demands of the Haber-Bosch loop are quite similar in all flowsheets, as already pointed out, in view of a higher hydrogen conversion in SOEC-based solutions (i.e., higher heat production in ammonia reactor) and a higher recycling flowrate in SR-based plant (i.e., higher heat recovered within the loop).

Focusing on the solid oxide cell operation, the electrical consumption ranges between ~6.5 and 7 kWh_{el}/kg NH_3 in all cases. Nevertheless, the cell set-up is different, working at the thermoneutral point in *SOEC + ASU + HB* and *SOEC + e-ASU + HB* plants and below it in *SOEC + HB* one, which requires further considerations before identifying the most feasible solution. The main effects are visible on the system thermal behaviour (isothermal vs. endothermal) and the stacked cell module size at a hydrogen constant produced amount. Indeed, the applied current density decrease leads to a significant rise in the cell number according to Faraday law, also in view of the current technical constraints on the maximum single cell area for material stability issues [76]. As shown in Fig. 8, SOEC specific energy consumption varies considering a single cell voltage below or above the thermoneutral voltage V_{th}. The electric demand has an increasing trend since the material resistances rise at high loads, while the heat demand including the steam generation and the

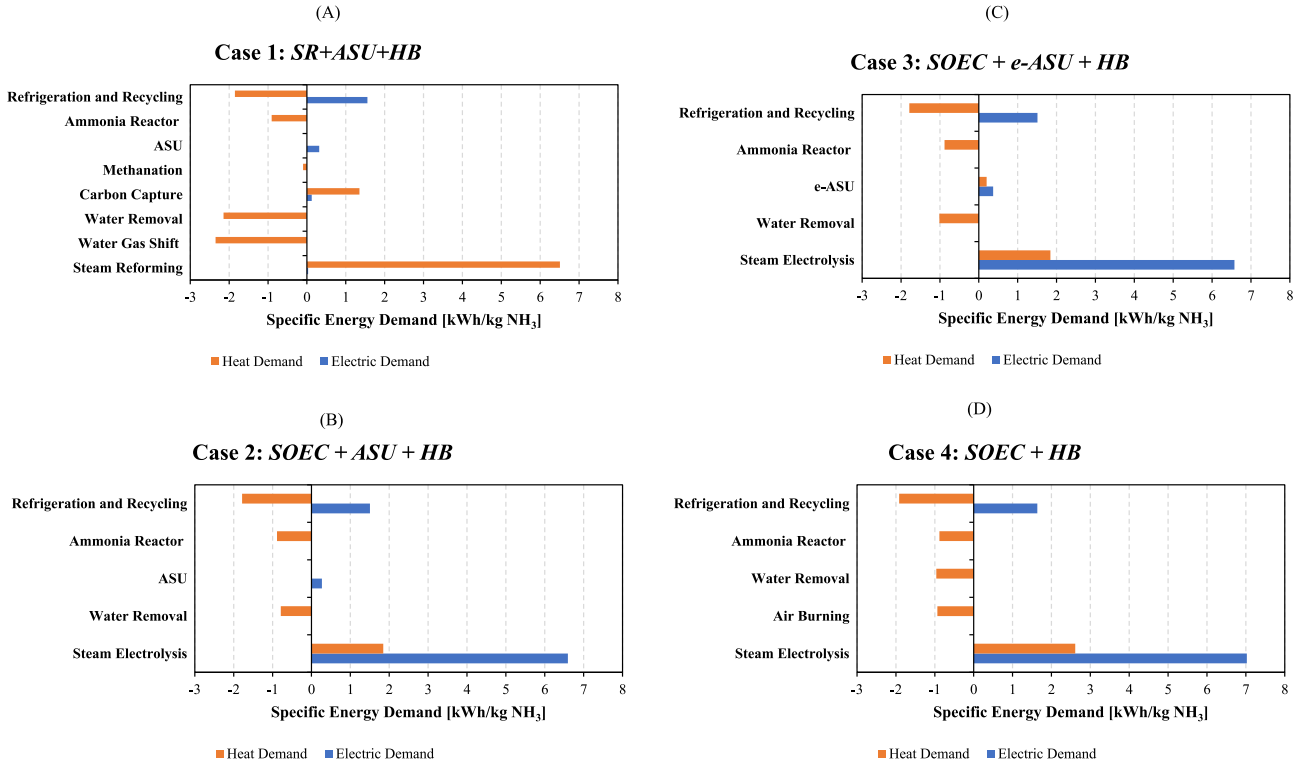

Fig. 7. Specific energy consumption in terms of electric work and heat for the unit operations involved in SR + ASU + HB (A), SOEC + ASU + HB (B), SOEC + e-ASU + HB (C) and SOEC + HB (D).

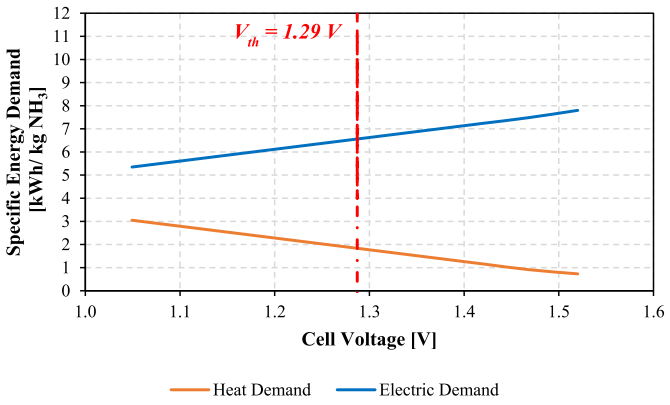

Fig. 8. SOEC specific energy consumption working below and upper the thermoneutral point.

cell effective operation decreases as less heat is required for a SOEC isothermal behaviour moving to the thermoneutral point and producing an excess heat after the thermoneutral point due to Joule effect. Fixed the nominal working at the thermoneutral point (6.6 kWh_{el}/kg NH_3, 1.85 kWh_{th}/kg NH_3 and 338250 stacked cells), a ~20% reduction of the cell voltage would allow for reaching a 5.35 kWh_{el}/kg NH_3 for the electrolyser module (7.11 kWh_{el}/kg NH_3 on the whole) but with a heat demand of 3.05 kWh_{th}/kg NH_3 and a six times higher number of stacked cells. This last condition makes the technology less competitive in view of SOEC current high capital costs [77]. On the other hand, an increase of the cell voltage up to 1.5 V would provoke a total specific electric consumption of more than 9 kWh_{el}/kg NH_3 (7.5 kWh_{el}/kg NH_3 due to the electrolyser) minimising almost all the benefits of using a high-temperature cell design, despite a lower cell module size and avoiding an external heat source. It is noteworthy that further material improvements, reducing the resistances, would permit a thermoneutral operation at higher currents by minimising the electrolyser size and consumption.

According to the solid oxide cell current performance, the *SOEC + HB* plant requires an almost double value of stacked cells with respect to *SOEC + ASU + HB,* working below the thermoneutral point and considering cells for the water re-reduction after air burning steps (which substitute the adsorption columns yet). The use of a devoted module as the oxygen separator leads to an increase also of ~27% of the total cell number in *SOEC + e-ASU + HB* case. Nevertheless, the attended SOEC price reduction according to an economy of scale should favour a wider commercial spread of dual operation cells which permit an easy modularity of the plant.

4. Conclusion

Since the Haber-Bosch process is the only available solution guaranteeing a quite high ammonia conversion and yield, the current industrial challenge consists of its decarbonization to make the products green. Among several proposed plant revamping strategies, Power-to-Ammonia approach results in the most promising alternative by permitting an easy coupling with renewables and the system scalability in view of the cell modularity. Knowing the huge electricity demand as the main issue for electrolysis applications, the work proposed and compared different plant designs exploiting the high-temperature solid oxide cell technology. Indeed, it has the unique property of working as both a water electrolyser and an oxygen separator. Four case-studies were discussed: (i) the state-of-art flowsheet involving the natural gas steam reforming and a traditional air separation unit as the commercial reference, (ii) a system with solid oxide electrolysis cell substituting the reformer and coupled with a traditional air separation unit, (iii) a system with two solid oxide cell modules devoted to the hydrogen (electrolysis operation) and the nitrogen (electrochemical air separation unit operation) production respectively, (iv) a solution with solid oxide cell stacks in series to air burners combining the water electrochemical reduction with the oxygen separation. In addition to minimising carbon emissions (~-1.4 kg CO_2/kg NH_3), all these alternatives show a lower energy demand (8.4–8.7 kWh/kg NH_3 vs 10.4 kWh/kg NH_3 of the steam reforming case). Moreover, an effective heat recovery within the plants permits the combination of the heat available from Haber-Bosch loop and the heat needed for inlet steam generation minimising the external hot requirements, also in view of a H_2O lower required amount with respect to the steam reforming (~-38%). Comparing the solid oxide cell-based plant set-ups, the specific operation differs significantly leading to an increasing number of stacked cells using additional modules both for the electrochemical air separation unit and in the dual function cell case (~30% and ~60% increase with respect to the basic flowsheet respectively). Currently a high number of stacked cells penalises economically the solid oxide cell use; the reduction in capital cost and the decrease in material resistances would make these green processes more competitive for a wide range of applications yet.

Funding

This research was developed within the project "Network 4 Energy Sustainable Transition – NEST" funded under the National Recovery and Resilience Plan (NRRP), Mission 4 Component 2 Investment 1.3 - Call for tender No. 1561 of 11.10.2022 of Ministero dell'Università e della Ricerca (MUR); funded by the European Union – NextGenerationEU.

CRediT authorship contribution statement

Fiammetta Rita Bianchi: Writing – review & editing, Writing – original draft, Visualization, Software, Methodology, Data curation, Conceptualization. **Barbara Bosio:** Writing – review & editing, Supervision, Methodology, Funding acquisition, Conceptualization.

Declaration of competing interest

The authors declare that they have no known competing financial interests or personal relationships that could have appeared to influence the work reported in this paper.

Nomenclature

A	Cell active area
E_a	Activation energy
E_{el}	Specific electric demand
E_{th}	Specific heat demand
F	Faraday constant
J	Current density
J_{lim}	Limiting current density
LHV	Lower Heating Value
n	Stacked cell number
N	Flowrate
P_{el}	Electric power
P_{th}	Thermal power
R_g	Ideal gas constant
T	Temperature
V	Voltage
V_{eq}	Equilibrium voltage
V_p	Overpotential
V_{th}	Thermoneutral voltage
y	Molar fraction
z	Charge number

Greek letters

γ	Pre-exponential coefficient
η	Efficiency

References

[1] Tornatore C, Marchitto L, Sabia P, De Joannon M. Ammonia as green fuel in internal combustion engines: state-of-the-art and future perspectives. Front Mech Eng 2022;8:1–16. https://doi.org/10.3389/fmech.2022.944201.

[2] Dhawale DS, Biswas S, Kaur G, Giddey S. Challenges and advancement in direct ammonia solid oxide fuel cells: a review. Inorg Chem Front 2023;10:6176–92. https://doi.org/10.1039/d3qi01557b.

[3] Zhao Y, Wang T, Setzler BP, Abbasi R, Wang J, Yan Y. A high-performance gas-fed direct ammonia hydroxide exchange membrane fuel cell. ACS Energy Lett 2021;6:1996–2002. https://doi.org/10.1021/acsenergylett.1c00370.

[4] Risso R, Cardona L, Archetti M, Lossani F, Bosio B, Bove D. A review of on-board carbon capture and storage techniques: solutions to the 2030 IMO regulations. Energies 2023;16. https://doi.org/10.3390/en16186748.

[5] Rouwenhorst KHR, Krzywda PM, Benes NE, Mul G, Lefferts L. Ammonia production technologies. Elsevier Inc.; 2021. https://doi.org/10.1016/b978-0-12-820560-0.00004-7.

[6] Pattabathula V, Richardson J. Introduction to ammonia production. Chem Eng Prog 2016;112:69–75. https://www.aiche.org/sites/default/files/cep/20160969.pdf.

[7] Lee K, Liu X, Vyawahare P, Sun P, Elgowainy A, Wang M. Techno-economic performances and life cycle greenhouse gas emissions of various ammonia production pathways including conventional, carbon-capturing, nuclear-powered, and renewable production. Green Chem 2022;24:4830–44. https://doi.org/10.1039/d2gc00843b.

[8] Olabi AG, Abdelkareem MA, Al-Murisi M, Shehata N, Alami AH, Radwan A, Wilberforce T, Chae KJ, Sayed ET. Recent progress in Green Ammonia: production, applications, assessment; barriers, and its role in achieving the sustainable development goals. Energy Convers Manag 2023;277:116594. https://doi.org/10.1016/j.enconman.2022.116594.

[9] Bird F, Clarke A, Davies P, Surkovic E. Ammonia : fuel and energy store. https://royalsociety.org/-/media/policy/projects/green-ammonia/green-ammonia-policy-briefing.pdf; 2020.

[10] Smith C, Hill AK, Torrente-Murciano L. Current and future role of Haber-Bosch ammonia in a carbon-free energy landscape. Energy Environ Sci 2020;13:331–44. https://doi.org/10.1039/c9ee02873k.

[11] Ammonia Technology Roadmap. Ammon. Technol. Roadmap 2021. https://doi.org/10.1787/f6daa4a0-en.

[12] IRENA and AEA. Innovation outlook: renewable ammonia. 2022. ISBN: 978-92-9260-423-3.

[13] Sousa J, Waiblinger W, Friedrich KA. Techno-economic study of an electrolysis-based green ammonia production plant. Ind Eng Chem Res 2022;61:14515–30. https://doi.org/10.1021/acs.iecr.2c00383.

[14] Qi M, Kim M, Dat Vo N, Yin L, Liu Y, Park J, Moon I. Proposal and surrogate-based cost-optimal design of an innovative green ammonia and electricity co-production system via liquid air energy storage. Appl Energy 2022;314:118965. https://doi.org/10.1016/j.apenergy.2022.118965.

[15] Bianchi FR, Bosio B. Operating principles, performance and technology readiness level of reversible solid oxide cells. Sustainability 2021;13:4777. https://doi.org/10.3390/su13094777.

[16] Ghaebi Panah P, Cui X, Bornapour M, Hooshmand RA, Guerrero JM. Marketability analysis of green hydrogen production in Denmark: scale-up effects on grid-connected electrolysis. Int J Hydrogen Energy 2022;47:12443–55. https://doi.org/10.1016/j.ijhydene.2022.01.254.

[17] Cameli F, Kourou A, Rosa V, Delikonstantis E, Galvita V, Van Geem KM, Stefanidis GD. Conceptual process design and technoeconomic analysis of an e-ammonia plant: green H_2 and cryogenic air separation coupled with Haber-Bosch process. Int J Hydrogen Energy 2023;49:1416–25. https://doi.org/10.1016/j.ijhydene.2023.10.020.

[18] Lee B, Lim D, Lee H, Lim H. Which water electrolysis technology is appropriate? Critical insights of potential water electrolysis for green ammonia production. Renew Sustain Energy Rev 2021;143:110963. https://doi.org/10.1016/j.rser.2021.110963.

[19] Ghavam S, Vahdati M, Wilson IAG, Styring P. Sustainable ammonia production processes. Front Energy Res 2021;9:1–19. https://doi.org/10.3389/fenrg.2021.580808.

[20] Garcia I, Cortazar M, Santamaria L, Lopez G, Bilbao J, Olazar M, Amutio M, Artetxe M. Biomass pyrolysis and in-line air–steam reforming as a potential strategy to progress towards sustainable ammonia production. Energy Convers Manag 2024;304:118221. https://doi.org/10.1016/j.enconman.2024.118221.

[21] Dziva G, Luan C, Ding G, Boré A, Jean Ives Kouakou K, Tembo T, Ullah A, Zaman M, Li S, Zeng L. Techno-economic analysis of small-scale ammonia production via sorption-enhanced gasification of biomass. Chem Eng J 2024;490. https://doi.org/10.1016/j.cej.2024.151666.

[22] MacFarlane DR, Cherepanov PV, Choi J, Suryanto BHR, Hodgetts RY, Bakker JM, Ferrero Vallana FM, Simonov AN. A roadmap to the ammonia economy. Joule 2020;4:1186–205. https://doi.org/10.1016/j.joule.2020.04.004.

[23] Giddey S, Badwal SPS, Kulkarni A. Review of electrochemical ammonia production technologies and materials. Int J Hydrogen Energy 2013;38:14576–94. https://doi.org/10.1016/j.ijhydene.2013.09.054.

[24] Xu G, Liu R, Wang J. Electrochemical synthesis of ammonia using a cell with a Nafion membrane and $SmFe_{0.7}Cu_{0.3-x}Ni_xO_3$ (x = 0-0.3) cathode at atmospheric pressure and lower temperature. Sci China, Ser B: Chem 2009;52:1171–5. https://doi.org/10.1007/s11426-009-0135-7.

[25] Liu R, Xu G. Comparison of electrochemical synthesis of ammonia by using sulfonated polysulfone and nafion membrane with $Sm_{1.5}Sr_{0.5}NiO_4$. Chin J Chem 2010;28:139–42. https://doi.org/10.1002/cjoc.201090044.

[26] Skodra A, Stoukides M. Electrocatalytic synthesis of ammonia from steam and nitrogen at atmospheric pressure. Solid State Ionics 2009;180:1332–6. https://doi.org/10.1016/j.ssi.2009.08.001.

[27] Goldstein V, Rath MK, Kossenko A, Litvak N, Kalashnikov A, Zinigrad M. Solid oxide fuel cells for ammonia synthesis and energy conversion. Sustain Energy Fuels 2022;6:4706–15. https://doi.org/10.1039/d2se00954d.

[28] van Langevelde PH, Katsounaros I, Koper MTM. Electrocatalytic nitrate reduction for sustainable ammonia production. Joule 2021;5:290–4. https://doi.org/10.1016/j.joule.2020.12.025.

[29] Atrashkevich A, Fajardo AS, Westerhoff P, Walker WS, Sánchez-Sánchez CM, Garcia-Segura S. Overcoming barriers for nitrate electrochemical reduction: by-passing water hardness. Water Res 2022;225. https://doi.org/10.1016/j.watres.2022.119118.

[30] Fan K, Xie W, Li J, Sun Y, Xu P, Tang Y, Li Z, Shao M. Active hydrogen boosts electrochemical nitrate reduction to ammonia. Nat Commun 2022;13:1–13. https://doi.org/10.1038/s41467-022-35664-w.

[31] Yang J, Wu A, Au SF, Yang Y, Huang X, Lei J, Liu Z, Zhang Y, Meng B, Lu Z, Guan W. One-step method to produce feedstock for green ammonia of H_2:N_2≥3:1 by solid oxide cell. Int J Hydrogen Energy 2024;56:1132–8. https://doi.org/10.1016/j.ijhydene.2023.12.264.

[32] Li R, Liu X, He G, Hu P, Zhen Q, Liu JL, Bashir S. Green catalytic synthesis of ammonia using solid oxide electrolysis cells composed of multicomponent materials. Catal Today 2021;374:102–16. https://doi.org/10.1016/j.cattod.2021.03.029.

[33] Bi W, Gyenge E, Wilkinson DP. Crossover, volatilization, and adsorption of ammonium ions in a proton-exchange membrane electrolyzer in relation to electrochemical ammonia production. Chem Eng J 2023;478. https://doi.org/10.1016/j.cej.2023.147359.

[34] Hirakawa H, Hashimoto M, Shiraishi Y, Hirai T. Photocatalytic conversion of nitrogen to ammonia with water on surface oxygen vacancies of titanium dioxide. J Am Chem Soc 2017;139:10929–36. https://doi.org/10.1021/jacs.7b06634.

[35] Lashgari M, Zeinalkhani P. Ammonia photosynthesis under ambient conditions using an efficient nanostructured FeS_2/CNT solar-energy-material with water feedstock and nitrogen gas. Nano Energy 2018;48:361–8. https://doi.org/10.1016/j.nanoen.2018.03.079.

[36] Shi Y, Zhao Z, Yang D, Tan J, Xin X, Liu Y, Jiang Z. Engineering photocatalytic ammonia synthesis. Chem Soc Rev 2023;52:6938–56. https://doi.org/10.1039/d2cs00797e.

[37] El-Shafie M, Kambara S. Recent advances in ammonia synthesis technologies: toward future zero carbon emissions. Int J Hydrogen Energy 2022. https://doi.org/10.1016/j.ijhydene.2022.09.061.

[38] Peng P, Chen P, Schiappacasse C, Zhou N, Anderson E, Chen D, Liu J, Cheng Y, Hatzenbeller R, Addy M, Zhang Y, Liu Y, Ruan R. A review on the non-thermal plasma-assisted ammonia synthesis technologies. J Clean Prod 2018;177:597–609. https://doi.org/10.1016/j.jclepro.2017.12.229.

[39] Bajpai A, Kumar S. Tailoring the surface acidity of catalyst to enhance nonthermal plasma-assisted ammonia synthesis rates. Mol Catal 2024;557:113961. https://doi.org/10.1016/j.mcat.2024.113961.

[40] Meloni E, Cafiero L, Martino M, Palma V. Structured catalysts for non-thermal plasma-assisted ammonia synthesis. Energies 2023;16:1–17. https://doi.org/10.3390/en16073218.

[41] Hollevoet L, Vervloessem E, Gorbanev Y, Nikiforov A, De Geyter N, Bogaerts A, Martens JA. Energy-efficient small-scale ammonia synthesis process with plasma-enabled nitrogen oxidation and catalytic reduction of adsorbed NO_x. ChemSusChem 2022;15. https://doi.org/10.1002/cssc.202102526.

[42] Sarafraz MM, Christo FC. Sustainable three-stage chemical looping ammonia production (3CLAP) process. Energy Convers Manag 2021;229:113735. https://doi.org/10.1016/j.enconman.2020.113735.

[43] Wang B, Yin X, Wang P, Shen L. Chemical looping ammonia synthesis at atmospheric pressure benefiting from synergistic effect of Mn- and Fe-based nitrogen carriers. Int J Hydrogen Energy 2023;48:2705–17. https://doi.org/10.1016/j.ijhydene.2022.10.132.

[44] Gao W, Wang R, Feng S, Wang Y, Sun Z, Guo J, Chen P. Thermodynamic and kinetic considerations of nitrogen carriers for chemical looping ammonia synthesis. Discov. Chem. Eng. 2023;3. https://doi.org/10.1007/s43938-023-00019-4.

[45] Wang B, Shen L. Recent advances in NH_3 synthesis with chemical looping technology. Ind Eng Chem Res 2022;61:18215–31. https://doi.org/10.1021/acs.iecr.2c02926.

[46] Schwalbe JA, Statt MJ, Chosy C, Singh AR, Rohr BA, Nielander AC, Andersen SZ, McEnaney JM, Baker JG, Jaramillo TF, Norskov JK, Cargnello M. A combined theory-experiment analysis of the surface species in lithium-mediated NH_3 electrosynthesis. Chemelectrochem 2020;7:1542–9. https://doi.org/10.1002/celc.201902124.

[47] Oshikiri T, Ueno K, Misawa H. Ammonia photosynthesis: via an association pathway using a plasmonic photoanode and a zirconium cathode. Green Chem 2019;21:4443–8. https://doi.org/10.1039/c9gc01658a.

[48] Cinti G, Frattini D, Jannelli E, Desideri U, Bidini G. Coupling solid oxide electrolyser (SOE) and ammonia production plant. Appl Energy 2017;192:466–76. https://doi.org/10.1016/j.apenergy.2016.09.026.

[49] Nowicki DA, Agnew GD, Irvine JTS. Green ammonia production via the integration of a solid oxide electrolyser and a Haber-Bosch loop with a series of solid electrolyte oxygen pumps. Energy Convers Manag 2023;280:116816. https://doi.org/10.1016/j.enconman.2023.116816.

[50] Mukelabai MD, Gillard JM, Patchigolla K. A novel integration of a green power-to-ammonia to power system: reversible solid oxide fuel cell for hydrogen and power production coupled with an ammonia synthesis unit. Int J Hydrogen Energy 2021; 46:18546–56. https://doi.org/10.1016/j.ijhydene.2021.02.218.
[51] Biswas S, Rathore SS, Kulkarni AP, Giddey S, Bhattacharya S. A theoretical study on reversible solid oxide cells as key enablers of cyclic conversion between electrical energy and fuel. Energies 2021;14. https://doi.org/10.3390/en14154517.
[52] Iyer S, Kaur G, Haque N, Giddey S. Review of experimental and modelling investigations for solid oxide electrolysis technology. Int J Hydrogen Energy 2024; 72:537–58. https://doi.org/10.1016/j.ijhydene.2024.05.312.
[53] Wang M, Nowicki KM, Irvine JTS. A novel solid oxide electrochemical oxygen pump for oxygen therapy. J Electrochem Soc 2022;169:064509. https://doi.org/10.1149/1945-7111/ac7008.
[54] Reisert M, Aphale A, Hu B, Heo SJ, Hong J, Singh P, Taylor D, Graf J. Solid state electrochemical oxygen separation and compression. Int. Conf. Environ. Syst. 2019 https://hdl.handle.net/2346/84625.
[55] Hansen JB, V Hendriksen P. Ammonia properties and its production. ECS Trans 2019;91:2455–65. https://doi.org/10.1149/09101.2455ecst.
[56] Zhang H, Wang L, Van herle J, Maréchal F, Desideri U. Techno-economic comparison of green ammonia production processes. Appl Energy 2020;259: 114135. https://doi.org/10.1016/j.apenergy.2019.114135.
[57] Liu Q, Su PC, Chan SH. Wet-air co-electrolysis in high-temperature solid oxide electrolysis cell for production of ammonia feedstock. Int J Hydrogen Energy 2022; 47:18577–86. https://doi.org/10.1016/j.ijhydene.2022.04.017.
[58] Ofori-Bah CO, Amanor-Boadu V. Directing the wind: techno-economic feasibility of green ammonia for farmers and community economic viability. Front Environ Sci 2023;10:1–16. https://doi.org/10.3389/fenvs.2022.1070212.
[59] Elishav O, Mosevitzky Lis B, Valera-Medina A, Grader GS. Storage and distribution of ammonia. Elsevier Inc.; 2020. https://doi.org/10.1016/B978-0-12-820560-0.00005-9.
[60] Bianchi FR, Bosio B, Conte F, Massucco S, Mosaico G, Natrella G, Saviozzi M. Modelling and optimal management of renewable energy communities using reversible solid oxide cells. Appl Energy 2023;334:120657. https://doi.org/10.1016/j.apenergy.2023.120657.
[61] Nosherwani SA, Neto RC. Techno-economic assessment of commercial ammonia synthesis methods in coastal areas of Germany. J Energy Storage 2021;34:102201. https://doi.org/10.1016/j.est.2020.102201.
[62] Ahn H, Luberti M, Liu Z, Brandani S. Process simulation of aqueous MEA plants for postcombustion capture from coal-fired power plants. Energy Proc 2013;37: 1523–31. https://doi.org/10.1016/j.egypro.2013.06.028.
[63] Wu Y, Xiang Y, Cai L, Liu H, Liang Y. Optimization of a novel cryogenic air separation process based on cold energy recovery of LNG with exergoeconomic analysis. J Clean Prod 2020;275:123027. https://doi.org/10.1016/j.jclepro.2020.123027.
[64] Syakdani A, Bow Y, Rusdianasari, Taufik M. Analysis of cooler performance in air supply feed for nitrogen production process using pressure swing adsorption (PSA) method. J. Phys. Conf. Ser. 2019;1167. https://doi.org/10.1088/1742-6596/1167/1/012055.
[65] Banaszkiewicz T, Chorowski M, Gizicki W. Comparative analysis of oxygen production for oxy-combustion application. Energy Proc 2014;51:127–34. https://doi.org/10.1016/j.egypro.2014.07.014.
[66] Hashim SS, Mohamed AR, Bhatia S. Oxygen separation from air using ceramic-based membrane technology for sustainable fuel production and power generation. Renew Sustain Energy Rev 2011;15:1284–93. https://doi.org/10.1016/j.rser.2010.10.002.
[67] Meixner DL, Brengel DD, Henderson BT, Abrardo JM, Wilson MA, Taylor DM, Cutler RA. Electrochemical oxygen separation using solid electrolyte ion transport membranes. J Electrochem Soc 2002;149:D132. https://doi.org/10.1149/1.1495908.
[68] Bianchi FR, Bosio B, Baldinelli A, Barelli L. Optimization of a reference kinetic model for solid oxide fuel cells. Catalysts 2020;10:104. https://doi.org/10.3390/catal10010104.
[69] Bianchi FR, Baldinelli A, Barelli L, Cinti G, Audasso E, Bosio B. Multiscale modeling for reversible solid oxide cell operation. Energies 2020;13:5058. https://doi.org/10.3390/en13195058.
[70] Asensio AM, Bianchi D, Rita Clematis Fiammetta, Bosio B, Barbucci A. A kinetic study on oxygen redox reaction of a double-perovskite reversible oxygen electrode—Part I: experimental analysis. JPhys Energy 2024;6:015011. https://doi.org/10.1088/2515-7655/ad0e29.
[71] Conti B, Bosio B, McPhail SJ, Santoni F, Pumiglia D, Arato E. A 2-D model for intermediate temperature solid oxide fuel cells preliminarily validated on local values. Catalysts 2019;9:36. https://doi.org/10.3390/catal9010036.
[72] Padinjarethil AK, Bianchi FR, Bosio B, Hagen A. Electrochemical characterization and modelling of anode and electrolyte supported solid oxide fuel cells. Front Energy Res 2021;9. https://doi.org/10.3389/fenrg.2021.668964.
[73] Irshad M, Siraj K, Raza R, Ali A, Tiwari P, Zhu B, Rafique A, Ali A, Ullah MK, Usman A. A brief description of high temperature solid oxide fuel cell's operation, materials, design, fabrication technologies and performance. Appl Sci 2016;6. https://doi.org/10.3390/app6030075.
[74] Bosio B, Bianchi FR. Multiscale modelling potentialities for solid oxide fuel cell performance and degradation analysis. Sustain Energy Fuels 2022;7:280–93. https://doi.org/10.1039/d2se01118b.
[75] Hauch A, Küngas R, Blennow P, Hansen AB, Hansen JB, Mathiesen BV, Mogensen MB. Recent advances in solid oxide cell technology for electrolysis. Science 2020:370. https://doi.org/10.1126/science.aba6118.
[76] Office of Energy Efficiency & Renewable Energy. Manufacturing cost analysis of 100 and 250 kW fuel cell systems for primary power and combined heat and power applications. https://www.energy.gov/eere/fuelcells/downloads/manufacturing-cost-analysis-100-and-250-kw-fuel-cell-systems-primary-power. [Accessed 24 March 2022].
[77] Anghilante R, Colomar D, Brisse A, Marrony M. Bottom-up cost evaluation of SOEC systems in the range of 10–100 MW. Int J Hydrogen Energy 2018;43:20309–22. https://doi.org/10.1016/j.ijhydene.2018.08.161.